Fabrication and Image Servo Tracking Study of a Continuum Robot Prototype

Ming-Hong Hsu, Phuc Thanh-Thien Nguyen, Dai-Dong Nguyen,
Toan-Khoa Nguyen, *Member, RST*, and Chung-Hsien Kuo*, *Member, RST*

***Abstract*— This study presents the design and implementation of a continuum manipulator associated with connected continuum kinematic modules (CKMs) to ease the fabrication of a continuum robot with multiple degrees of freedom. The proposed CKM consists of five sequential circular plates connected by universal joints, individual actuated tension cables surrounded by compression springs. All tension cables are controlled via linear actuators at a distal site. Consequently, a continuum robot is formed with three CKMs to demonstrate the feasibility of the proposed CKM via the Jacobian-based image servo tracking tasks. Finally, quantitative tracking error analyses are provided for the evaluation of the overall performance.**

Index Terms*— *Continuum Robot, Image Servo Tracking, Jacobian Image, Autonomous Manipulation.

I. Introduction

Robotic manipulators have been successfully used in a wide range of industrial, service, and medical applications. In addition to generally articulated manipulators, soft and flexible manipulators are getting more attractive to robotics researchers. The continuum robot is the typical example of flexible manipulators, performing better agility than conventional articulated manipulators. In general, continuum robots (Fig. 1.) simulate the manipulations of octopus tentacles for performing soft grasping and manipulating tasks. Hence, continuum robots are often employed to operate in narrow spaces because of hyper degrees of freedom (DOF) motions.

There are two main types in the design of continuum robots: tension cable-driven and pneumatic-driven. While the pneumatic-driven continuum robot needs a complicated pneumatic source for operation, the tension cable-driven robot usually uses motors or linear actuators as the source of kinematic motion control, taking advantage of installation, mobility, and maintenance. However, the kinematics of the tension cable-driven continuum robot is much complicated than the conventional articulated robot. Therefore, an ideal constant curvature assumption [1], [2] is often given for the derivation of continuum kinematics.

This study mainly focuses on developing a continuum kinematic module-based (CKM-based) approach for continuum robot design. Such a design paradigm is convenient for fabricating a continuum robot and efficiently obtaining the overall kinematic model for control purposes. Besides the design and control of the CKM-based continuum robot, the experiments for image servoing path tracking under Eye-to-Hand (ETH) configuration are also arranged to demonstrate the autonomous manipulation ability of the hyper DOF continuum manipulator, which is the possible deployment of service robot to provide manipulation compliance and ensure operator safety when performing the human-robot interaction (HRI).

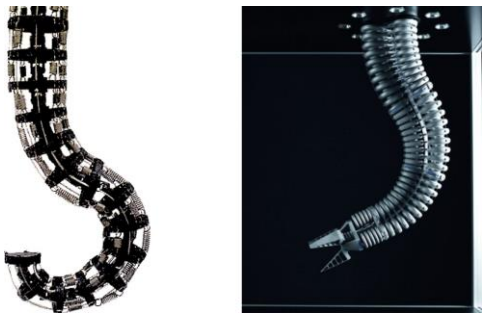

Fig. 1. Elephant's Trunk Manipulator [1] and Festo Bionic Handling Assistant [28].

II. Related Works

In recent years, automation-related equipment has been fast developed, especially robotic manipulators in various fields. Among various robotics manipulators, the development of continuum robots is getting popular because of their abilities in agility and compliance. Hannan et al. [1] proposed a continuum robot design, and their continuum robot is formed as 32 coupled joints with a total of 8 actuatable cables. Hence, their continuum robot can perform a motion similar to the elephant's trunk. However, the truck arc length and curvature used for the kinematics should be based on an ideal constant curvature. Therefore, the kinematics of bending motion could be derived in terms of the popular Denavit Hartenberg parameters. Then, Jones et al. [2] further proposed the method of synthesizing the kinematic relationship between a general continuum skeleton and a continuum robot. The coordinates are related to the controller's input (e.g., air pressure and tendon length) to realize real-time tasks and shape control of a continuum robot. There are also springs as the backbone of the disk connection, as proposed by Yoon et al. [3]. Such mechanism design is mainly used to enhance the elasticity and flexibility of the overall continuum structure to ensure the safety of the continuum robot when it collides with the human body. Another design [4] used elastic center column and springs, where the springs are installed

This work was finically supported by the Ministry of Science and Technology, Taiwan, R.O.C. under Grant MOST 109-2221-E-011-112-MY3. *(Corresponding author: Chung-Hsien Kuo)*

M.H Hsu, P.T.T. Nguyen, D.D. Nguyen, T.K. Nguyen are with the Department of Electrical Engineering, National Taiwan University of Science and Technology, Taipei, 106 Taiwan (e-mails: a0981757196@gmail.com; d10907813@mail.ntust.edu.tw; daidongnguyen9@gmail.com; toankhoabk@gmail.com).

C.H. Kuo is with the Department of Mechanical Engineering, National Taiwan University, Taipei, 106 Taiwan (e-mail: chunghsien@ntu.edu.tw).

outside the center column to avoid unexpected shapes such as twisting. Such a design is beneficial for handling weights and loads on the end effector; hence their continuum robot is demonstrated for the automatic harvesting tasks.

The uses of pneumatic artificial muscles are also available to develop continuum robots. Liu et al. [5] presented a light soft manipulator, and the thin McKibben pneumatic artificial muscles are utilized for continuously controllable stiffness actuation. Their study successfully overcomes the problem that most continuum robots cannot constantly change their stiffness at a fixed end position. Dalvand et al. [6] proposed an analytical loading model by considering the number of tendons and the load distribution of the tendons. The analytical loading model applies to the N-tendon configured continuum robots. Their study reported that the analytical loading model is promising in avoiding tendon relaxation, leading to inaccurate motion control.

Moreover, the bio-inspired continuum robot designs have impressive performance. For instance, Hassan et al. [7] developed an active-braid design to fabricate a bioinspired continuum manipulator. Their study adopted flexible cross-linked spiral array structures to form the continuum structure.

III. Design And Assembly

A. Robot Design

1) Continuum KinematicModule (CKM) Design

The continuum kinematic module (CKM) is formed from rigid plates (100 mm diameter, 5mm thickness). Fig. 2(b) shows that each CKM contains five circular plates combined with four connecting universal joints. Because the universal joints have a high degree of stiffness and lack elasticity, a compression spring with a diameter of 20mm is added to the outer of the universal joint to increase its elasticity and support. Additionally, the others spring is installed at the symmetrical position of the control cable position. Fig. 2(a) shows the positions L1, L2, L2 of the control cable and the positions L4, L5, L6 of the support spring.

2) *Actuation System*

To adapt the payload requirement and the stability of the tension cables during the robot operation process. The NiMotion SWU series of the sliding actuator with model SWUZ1204-200-A2-485 were selected. This study implements the continuum robot with three CKMs. Each CKM has three tension cables. Therefore, the actuation system requires nine sliding actuators arranged in 3x3 square with three sliding actuators in each control layer, as illustrated in Fig. 3.

B. Assembly of Continuum Manipulator

The proposed continuum manipulator consists of three CKM and the linear actuation system. Fig. 4. visualizes the assembly of the continuum robot, with the total length of the continuum spine is 670mm, and the fixed segment between CKM1 and CKM2 is 90mm and 70 mm correspondingly for the value of the fixed segment between CKM2 and CKM3.

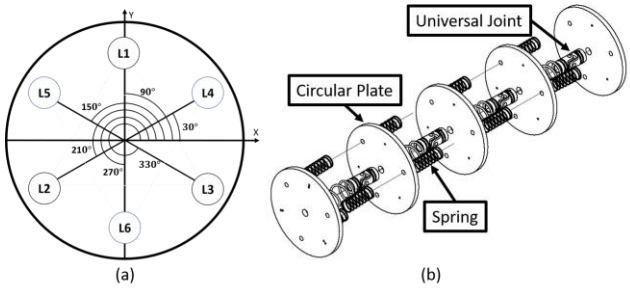

Fig. 2. (a) Compression spring and tension cables position; (b) CKM structure.

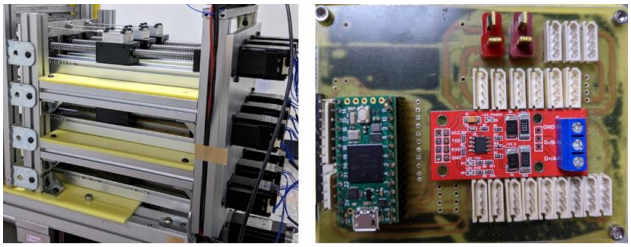

Fig. 3. a) Actuation system; b) Control circuit board.

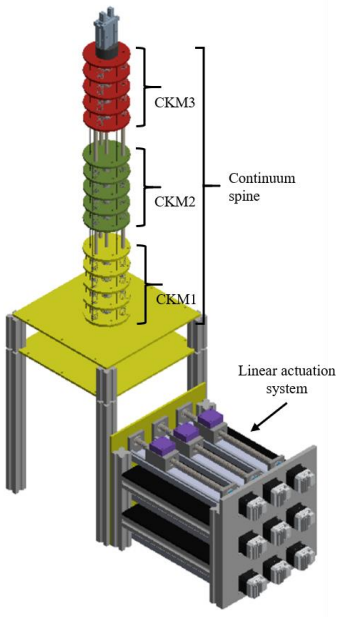

Fig. 4. Robot assembly.

IV. Kinematic Analysis

In this section, this study presents the kinematic of continuum manipulator, including three subsections: the continuum kinematic modules (CKM) analysis, the kinematic analysis of continuum manipulator, and the velocity kinematic analysis.

$$\begin{bmatrix} cos^2\varphi(cos\,\kappa l-1)+1 & sin\,\varphi\,cos\,\varphi(cos\,\kappa l-1) & cos\,\varphi\,sin\,\kappa l & \frac{cos\,\varphi(1-cos\,\kappa l)}{\kappa} \\ sin\,\varphi\,cos\,\varphi(cos\,\kappa l-1) & cos^2\varphi(1-cos\,\kappa l)+cos\,\kappa l & sin\,\varphi\,sin\,\kappa l & \frac{sin\,\varphi(1-cos\,\kappa l)}{\kappa} \\ -cos\,\varphi\,sin\,\kappa l & -sin\,\varphi\,sin\,\kappa l & cos\,\kappa l & \frac{sin\,\kappa l}{\kappa} \\ 0 & 0 & 0 & 1 \end{bmatrix} \quad (2)$$

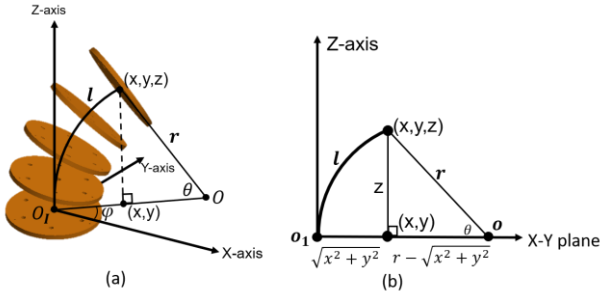

Fig. 5. The simulated posture of a single CKM reaching the target point (x, y) in 3-dimension **(a)** and 2-dimension **(b).**

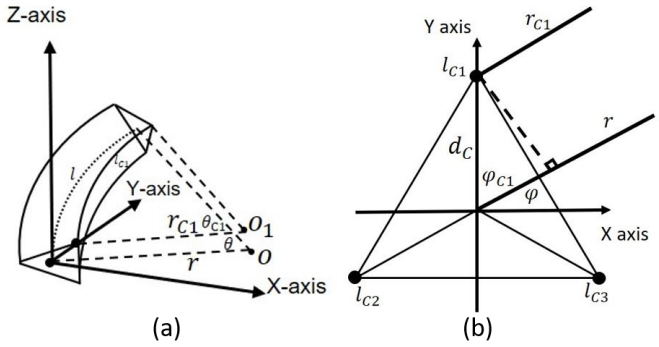

Fig. 6. The relationship between tension cables and arc parameters (φ, κ, l) in 3-dimension **(a)** and 2-dimension **(b).**

A. Continuum Kinematic Modules (CKM) Analysis

1) Forward Kinematic

Based on [1], we also assume that CKM bends as an ideal arc shape. Let arc parameters as (φ, κ, l), where l is the arc length of the centerline, r is the radius of arc, θ is the angle of arc, κ is the curvature of arc, and φ is the angle of CKM rotation on the x-y plane, as depicted in Fig. 5. Then, based on the D-H table (Table I), the transformation matrix from the center coordinate of the bottom circular plate to the center coordinate of the end circular plate can be obtained as following Eq. (1) and (2):

$$T_1^5 = T_1\,T_2\,T_3\,T_4\,T_5 \quad (1)$$

TABLE I
D-H PARAMETERS FOR THE CKM

Link	θ	h	a	α
1	φ	0	0	π/2
2	$\kappa l/2$	0	0	$-\pi/2$
3	0	$2/\kappa \sin(\kappa l/2)$	0	π/2
4	$\kappa l/2$	0	0	$-\pi/2$
5	$-\varphi$	0	0	0

2) Inverse Kinematic

As shown in Fig. 5, the target point (x, y) can be projected from three-dimensional space to two-dimensional space, and the angle φ can be obtained as the following formula:

$$\varphi = \tan^{-1}\frac{y}{x} \quad (3)$$

Due to a single CKM bends in an ideal arc shape, the intersection of the end circular plate and the bottom circular plate extension line is the center of the arc of the CKM centerline. Then the connecting line from the bottom circular plate to the center of the arc O through the projected target point (x, y). Based on the geometric relationship between the arc radius r and the endpoint (x, y, z), r and θ can be obtained as follows:

$$r = \frac{x^2+y^2+z^2}{2\sqrt{x^2+y^2}} \quad (4)$$

$$\theta = \cos^{-1}\left(\frac{r-\sqrt{x^2+y^2}}{r}\right) \quad (5)$$

The arc curvature κ is considered the reciprocal of the arc radius r as Eq. (6), and the arc length l of the centerline of the CKM can be obtained through the arc radius r and the arc angle θ, as Eq. (7):

$$\kappa = \frac{1}{r} \quad (6)$$

$$l = r\theta = \frac{cos^{-1}\left(1-\kappa\sqrt{x^2+y^2}\right)}{\kappa} \quad (7)$$

3) Parameter Conversion

Because tension cables are mainly controlled by linear actuators to manipulate CKMs, the arc parameters (φ, κ, l) need to be converted into the length of each tension cable to control CKMs. At present, the position of the tension cable is one of the three vertices of the equilateral triangle, so the arc length of the centerline of CKM is the average length of the three control cables:

$$l = \frac{l_{C1}+l_{C2}+l_{C3}}{3} \quad (8)$$

From Fig. 6(b), it can be found that $\varphi_{C1} = 90° - \varphi$, and the relation between φ_{C2} 、 φ_{C3} and the rotation angle φ of the CKM in the x-y plane can be deduced through the geometric relation:

$$\varphi_{C2} = 210° - \varphi \quad (9)$$

$$\varphi_{C3} = 330° - \varphi \quad (10)$$

The arc radius of the tension cable r_{C1} and the central arc radius r are two parallel lines, therefore, the relation between r_{C1} and r can be obtained through the trigonometric function:

$$r = r_{C1} + d_C * \cos\varphi_{C1} \quad (11)$$

where d_C is the distance between each cable to the center of the circular plate. Then each arc radius of tension cables r_{Ci} can be derived from the relation with the central arc radius r:

$$r_{Ci} = r - d_C \cos\varphi_{Ci}, i = 1\sim3 \quad (12)$$

$$l_{Ci} = r_{Ci}\theta \quad (13)$$

Finally, through Eq. (12) and (13), the arc length of each tension cable can be deduced as follows:

$$l_{Ci} = l - \theta d_C \cos\varphi_{Ci}, i = 1\sim3 \quad (14)$$

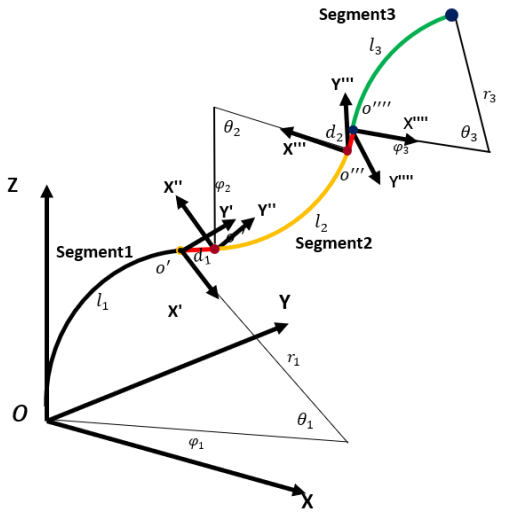

Fig. 7. The coordinate system of the continuum manipulator.

B. The Kinematic Analysis of Continuum Manipulator

According to the mechanical configuration, the relationship of the coordinate system of three CKM segments is shown in Fig. 7. The coordinate system of the first and third CKM is in the same direction, while the coordinate system of the second CKM is 180° different from the two others. Each CKM segment is calculated independently. The transformation matrix of the continuum manipulator is presented as follows:

$$T_m = T_{s_1}T_{d_1}T_{s_2}T_{d_2}T_{s_3} = \begin{bmatrix} a_{11} & a_{12} & a_{13} & a_{14} \\ a_{21} & a_{22} & a_{23} & a_{24} \\ a_{31} & a_{32} & a_{33} & a_{34} \\ a_{41} & a_{42} & a_{43} & a_{44} \end{bmatrix} \quad (15)$$

where the CKM transformation matrixT_{s_i} is defined as Eq. (2), the fixed segment transformation matrix T_{di} is defined as:

$$T_{d_i} = \begin{bmatrix} -1 & 0 & 0 & 0 \\ 0 & -1 & 0 & 0 \\ 0 & 0 & 1 & d_i \\ 0 & 0 & 0 & 1 \end{bmatrix} \quad (16)$$

with d_i is the length of a fixed segment.

C. Velocity Kinematic Analysis

According to Hannan et al. [1], velocity kinematic can be written as:

$$v_{jacobian} = [v_x \quad v_y \quad v_z \quad \omega_x \quad \omega_y \quad \omega_z]^T = \dot{x}_t = J\dot{q} \quad (17)$$

where $v_{jacobian}$ is the velocity of the End-effector, $\dot{x}_t$ implies the differential of x_t, which is position and vector in the task space, J is the Jacobian matrix and $\dot{q}$ is the change of the arc parameters of each axis:

$$\dot{q} = [\dot{\varphi}_1 \ \dot{k}_1 \ \dot{l}_1 \ \dot{\varphi}_2 \ \dot{k}_2 \ \dot{l}_2 \ \dot{\varphi}_3 \ \dot{k}_3 \ \dot{l}_3]^T \quad (18)$$

Hannan et al. [1] proposed the calculation method that the velocity kinematic needs to be calculated by the endpoint x_t. The endpoint x_t is mainly derived from the forward kinematics of the continuum manipulator to obtain $\dot{x}_t$ that is differentiated by chain rule:

$$\dot{T}_{s_1}^{s_3} = \dot{T}_{s_1}T_{d_1}^{s_3} + T_{s_1}\dot{T}_{d_1}T_{s_2}^{s_3} + T_{s_1}^{d_1}\dot{T}_{s_2}T_{d_2}^{s_3} + T_{s_1}^{s_2}\dot{T}_{d_2}T_{s_3} + T_{s_1}^{d_2}\dot{T}_{s_3} \quad (19)$$

or

$$\dot{T}_{s_1}^{s_3} = \begin{bmatrix} \alpha_{11} & \alpha_{12} & \alpha_{13} & \alpha_{14} \\ \alpha_{21} & \alpha_{22} & \alpha_{23} & \alpha_{24} \\ \alpha_{31} & \alpha_{32} & \alpha_{33} & \alpha_{34} \\ \alpha_{41} & \alpha_{42} & \alpha_{43} & \alpha_{44} \end{bmatrix} \quad (20)$$

Then, J$\dot{q}$ can be constructed as the last column of (20):

$$\mathrm{J}\dot{q} = [\alpha_{14} \quad \alpha_{24} \quad \alpha_{34}]^T \quad (21)$$

It is noted that $v_{jacobian}$ includes linear velocity and angular velocity. Therefore, the estimated position of the endpoint can be rewritten as $x_t = [x \quad y \quad z \quad \theta_t]^T$. Because of the structure limitation, it cannot rotate on the z-axis, so θ_z is not included in rotation vector. Thus, $\theta_t = [\theta_x \quad \theta_y]^T$ is the orientation angle of tangent vector t and can be obtained as follows:

$$\theta_t = \begin{bmatrix} arctan\frac{t_y}{t_z} \\ arctan\frac{t_x}{t_z} \end{bmatrix} \quad (21)$$

where the tangent vector t is defined as the third column of (20). Time derivative of θ_t can be defined as:

$$\dot{\theta}_t = \begin{bmatrix} \frac{\dot{t_y}t_z - t_y\dot{t_z}}{t_z^2+t_y^2} \\ \frac{\dot{t_x}t_z - t_x\dot{t_z}}{t_z^2+t_x^2} \end{bmatrix} \quad (23)$$

Also, the time derivative of tangent vector t can be defined as:

$$\dot{t} = J_t\dot{q} = \begin{bmatrix} \alpha_{13} \\ \alpha_{23} \\ \alpha_{33} \end{bmatrix} \quad (24)$$

where J_t is the position part of the Jacobian matrix for the tangent vector t. On the other hand, the rotation part of the Jacobian matrix can be computed as follows:

$$J_\theta = \begin{bmatrix} J_{\theta_1} \\ J_{\theta_2} \end{bmatrix} = \begin{bmatrix} \frac{1}{t_z^2+t_y^2}(t_zJ_{t2} - t_yJ_{t3}) \\ \frac{1}{t_z^2+t_x^2}(t_zJ_{t1} - t_xJ_{t3}) \end{bmatrix} \quad (25)$$

Finally, the velocity kinematic can be rewritten by combining Eq. (24) and (25):

$$v_{jacobian} = \begin{bmatrix} v_x \\ v_y \\ v_z \\ \omega_x \\ \omega_y \end{bmatrix} = \dot{\mathrm{x}} = \mathrm{J}\dot{q} = \begin{bmatrix} \alpha_{14} \\ \alpha_{24} \\ \alpha_{34} \\ J_{\theta_1}\dot{q} \\ J_{\theta_2}\dot{q} \end{bmatrix} \tag{26}$$

The Jacobian matrix associated with the forward kinematic can control the posture of the manipulator by the velocity and direction of the endpoint. When velocity kinematic is given, the variation of each arc parameter $\dot{q}$ can be obtained as follows:

$$\dot{q} = J(q)^{+}\dot{\mathrm{x}}_t + \{I - J(q)^{+}J(q)\}\varepsilon \tag{27}$$

where $J(q)^{+}$ is the pseudo inverse of the Jacobian matrix

$$J^{+} = W^{-1}J'(JW^{-1}J')^{-1} \tag{28}$$

with W is the identity matrix. The solution obtained by $J^{+}\dot{\mathrm{x}}_t$ is the least square solution, and $\{I - J(q)^{+}J(q)\}\varepsilon$ is the zero-space projection matrix. Then, the arc parameters of each KCM segment are obtained from Eq. (18) and the End-effector velocity. Finally, the length of the tension cables of each segment can be calculated through Eq. (8).

V. Experiments And Results

A. *Simulation Analysis of Kinematics*

In this section, the correctness of the kinematics and the manipulator posture are verified by simulation in MATLAB. To analyze the manipulator kinematic, we mainly change the arc parameters (κ, φ, l) in different simulation cases and show in Fig. 9, Fig. 10, and Fig. 11.

As the results are shown in Table II, the position errors in the x- and y-direction are within 10mm, while the position errors in the z-direction are under 50mm, proving the feasibility of CKM kinematic in the designed continuum manipulator.

TABLE II
End Point Error of Continuum Manipulator Posture in The Velocity Kinematic Simulation

Speed variation	20mm/s in Y direction					
	X	Y	Z	Y error	Y error	Z error
Start point	279.6	-101.5	586.8			
Try 1	281.4	-79.38	591	-1.8	-2.12	-4.2
Try 2	282.7	-57.43	594.4	-3.1	-4.07	-7.6
Try 3	283.5	-36.03	596.8	-3.9	-5.47	-10
Try 4	283.6	-16.42	598.3	-4	-5.08	-11.5
Speed variation	20mm/s in X direction					
Start point	279.6	-101.5	586.8			
Try 1	298.4	-103.5	575.5	1.2	-2	11.3
Try 2	316.7	-105.3	563.3	2.9	-3.8	23.5
Try 3	334.3	-106.7	551.2	5.3	-1.4	35.6
Try 4	351.2	-107.7	538.4	8.4	-2.4	48.4

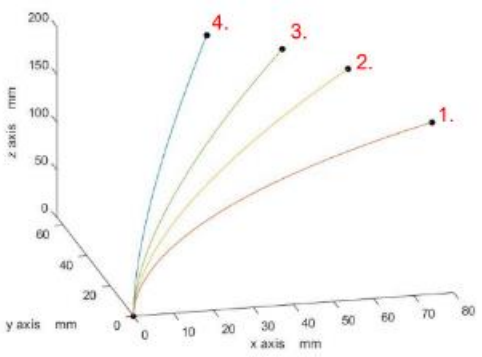

Fig. 8. Simulation of single CKM kinematic, with fixed arc curvature κ and arc length l values, with 0.003 and 170, respectively, while rotation angle φ is changed in {0, π/6, π/4, π/3} corresponding 1-4 curves.

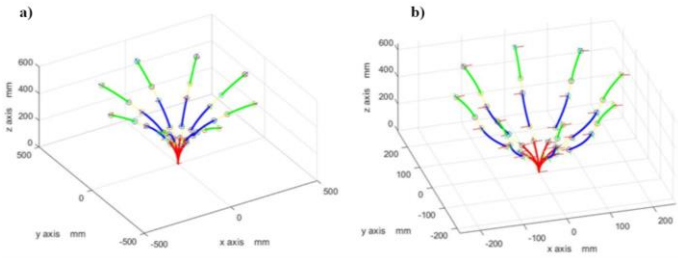

Fig. 9. The rotation angle changing simulation of the continuum manipulator kinematic in three segments with fixed arc curvature κ of three segments is 0.003, 0.002, 0.001 in order. **a)** The rotation angle φ is modified in the first segment and the third segment. **b)** Same rotation angle φ in three segments.

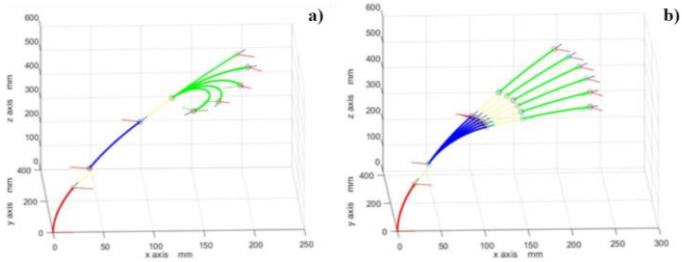

Fig. 10. Arc curvature changing simulation of the continuum manipulator kinematic in three segments with fixed rotation angle φ of three segments is π/3, 4π/3 and π/3 in order. **a)** The arc curvature κ is modified in the second segment. **b)** The arc curvature κ is modified in the third segment.

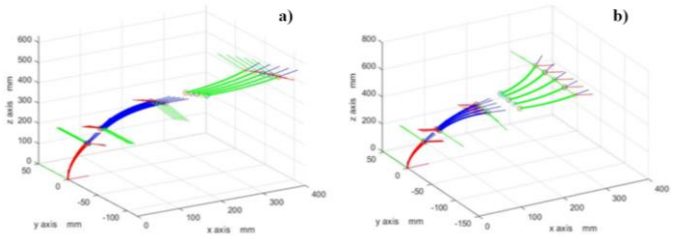

Fig. 11. Velocity kinematic of continuum manipulator. **a)** The velocity moves 20mm per second in the y-direction. **b)** The velocity moves 20mm per second in the x-direction.

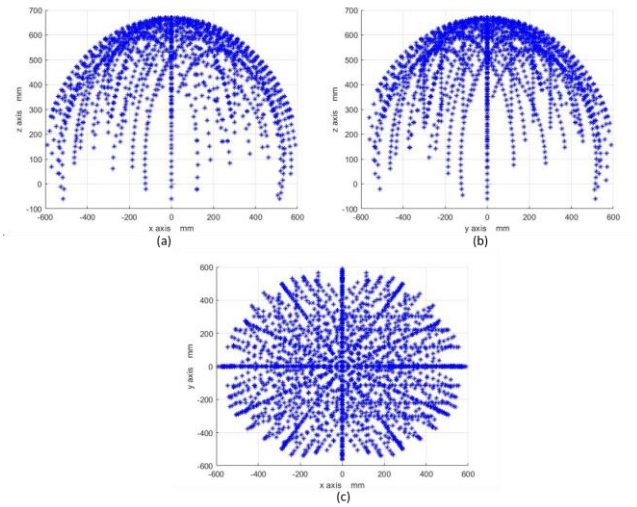

Fig. 12. Velocity kinematic of the continuum manipulator.

B. Working Space Analysis

Table III shows the operating range of the arc parameters. First, the current endpoint position of the manipulator can be obtained through modifying arc parameters (φ, κ, l) in the forward kinematic. Then the operating range of continuum manipulator in the ideal situation can be obtained. Nevertheless, the actual length of the compression springs is limited by ±20mm. Thus, the actual operating range of the manipulator can be obtained, as shown in Fig. 12.

TABLE III
WORKING RANGE OF ARC PARAMETERS

Parameter	$\theta_1, \theta_2, \theta_3$	$\varphi_1, \varphi_2, \varphi_3$	$\kappa_1, \kappa_2, \kappa_3$
Range	$0 \sim \pi/2$	$0 \sim \pi$	R^+

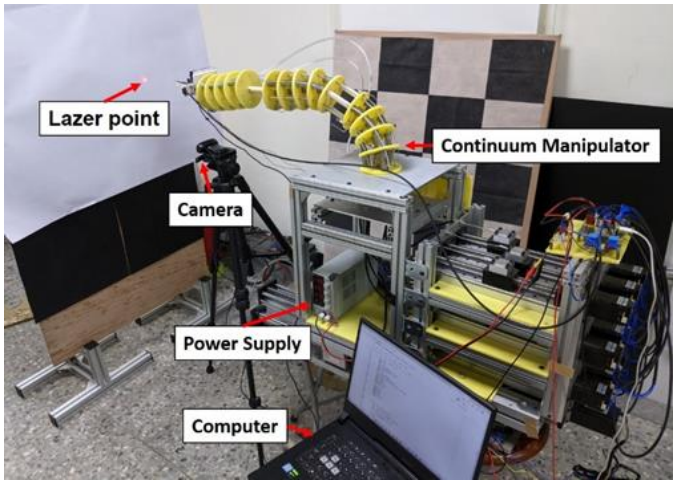

Fig. 13. The environment of trajectory tracking.

C. Heart Shape Trajectory Tracking

In this experiment, the trajectory tracking task of eye-to-hand (ETH) is used to verify the effectiveness of the Jacobian control method. First, in the experimental environment, as shown in Fig. 13, the camera position is fixed, and the distance from the laser point in the imaging screen is 0.23m. Then, different tracking points are generated in the image plane with the same heart shape size, as illustrated in Fig. 14. The image plane's tracking points and laser point position are then transferred to the manipulator coordinate system. Finally, the manipulator achieves trajectory tracking through velocity kinematics. The reference trajectory is the heart shape trajectory point defined in the image plane, and the estimated trajectory point is calculated by:

$$y = 60 - 20 \times \left(\arccos\left(1 - \frac{x}{40}\right) - \pi\right) \tag{29}$$

The error is the root mean square of the distance between the currently estimated laser points and the corresponding target points. The experimental results (Table II) show that the proposed control method can achieve accurate path tracking.

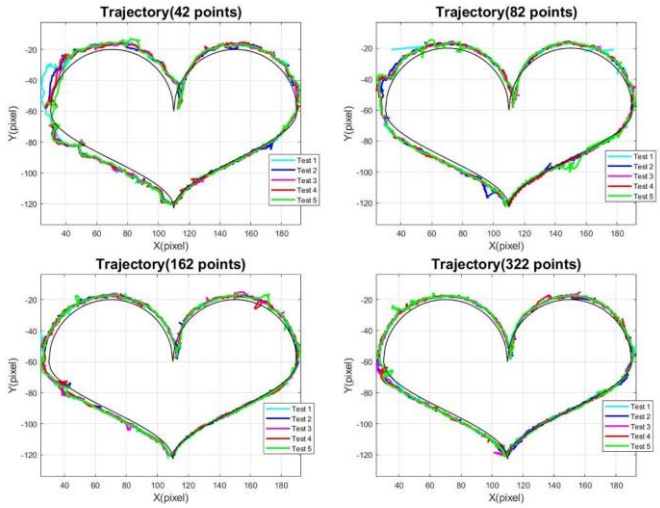

Fig. 14. Heart tracking trajectory with different tracking points. The black line is the reference path.

TABLE IV
RESULTS OF TRACKING ERROR IN DIFFERENT AMOUNT OF TRACKING POINTS

Number of points	Root Mean Square Error (RMSE)
42	7.74
82	6.08
162	4.30
322	4.03

VI. CONCLUSION

This study proposed connected continuum kinematic modules (CKMs) to ease the fabrication of the continuum manipulator with multiple degrees of freedom. The kinematics of the proposed continuum manipulator is verified through kinematic simulation and analysis. Furthermore, the ETH heart shape tracking experiment verifies the correctness of the kinematics and the accuracy of the manipulator control. Because the continuum manipulator has a greater degree of freedom and the wire-driven manipulator is susceptible to the influence of gravity and causes posture deviation, in future research, an inertial measurement unit (IMU) could be installed to correct the posture deviation through feedback. Furthermore, a PBVS-based image servo tracking could also be deployed to improve the accuracy of image servo tracking in the continuum manipulator, allowing the manipulator to perform more diversified tasks.

REFERENCES

[1] M. W. Hannan, and I. D. Walker, "Kinematics and the implementation of an elephant's trunk manipulator and other continuum style robots", *J. Robot. Syst*, vol. 20, pp. 45-63, 2003

[2] B. A. Jones, and I. D. Walker, "Kinematics for multisection continuum robots," *IEEE Transactions on Robotics*, vol. 22, no. 1, pp. 43-55, 2006

[3] H. S. Yoon, and B. J. Yi, "A 4-DOF flexible continuum robot using a spring backbone," *International Conference on Mechatronics and Automation*, pp. 1249-1254, 2009

[4] T. Tokunaga, K. Oka, and A. Harada, "1segment continuum manipulator for automatic harvesting robot - prototype and modeling," *IEEE International Conference on Mechatronics and Automation (ICMA)*, pp. 1655-1659, 2017

[5] Y. Liu, Y. Yang, Y. Peng, S. Zhong, N. Liu, and H. Pu, "A Light Soft Manipulator With Continuously Controllable Stiffness Actuated by a Thin McKibben Pneumatic Artificial Muscle," *IEEE/ASME Transactions on Mechatronics*, vol. 25, no. 4, pp. 1944-1952, 2020

[6] M. M. Dalvand, S. Nahavandi, and R. D. Howe, "An Analytical Loading Model for n-Tendon Continuum Robots," *IEEE Transactions on Robotics*, vol. 34, no. 5, pp. 1215-1225, 2018

[7] T. Hassan, M. Cianchetti, B. Mazzolai, C. Laschi, and P. Dario, "Active-Braid, a Bioinspired Continuum Manipulator," *IEEE Robotics and Automation Letters*, vol. 2, no. 4, pp. 2104-2110, 2017

[8] F. J. Comin, C. M. Saaj, S. M. Mustaza, and R. Saaj, "Safe Testing of Electrical Diathermy Cutting Using a New Generation Soft Manipulator," *IEEE Transactions on Robotics*, vol. 34, no. 6, pp. 1659-1666, 2018

[9] B. Zhao, W. Zhang, Z. Zhang, X. Zhu, and K. Xu, "Continuum Manipulator with Redundant Backbones and Constrained Bending Curvature for Continuously Variable Stiffness," *IEEE/RSJ International Conference on Intelligent Robots and Systems (IROS)*, pp. 7492-7499, 2018

[10] T. Qu, J. Chen, S. Shen, Z. Xiao, Z. Yue, and H. Y. K. Lau, "Motion control of a bio-inspired wire-driven multi-backbone continuum minimally invasive surgical manipulator," *IEEE International Conference on Robotics and Biomimetics (ROBIO)*, pp. 1989-1995, 2016

[11] M. Hwang, and D. Kwon, "Strong Continuum Manipulator for Flexible Endoscopic Surgery," *IEEE/ASME Transactions on Mechatronics*, vol. 24, no. 5, pp. 2193-2203, Oct. 2019

[12] S. Zhang, Q. Li, H. Yang, J. Zhao, and K. Xu, "Configuration Transition Control of a Continuum Surgical Manipulator for Improved Kinematic Performance," *IEEE Robotics and Automation Letters*, vol. 4, no. 4, pp. 3750-3757, 2019

[13] L. Wu, R. Crawford, and J. Roberts, "Dexterity Analysis of Three 6-DOF Continuum Robots Combining Concentric Tube Mechanisms and Cable-Driven Mechanisms," *IEEE Robotics and Automation Letters*, vol. 2, no. 2, pp. 514-521, 2017

[14] T. Wang et al., "Design and Analysis of a Snake-like Surgical Robot with Continuum Joints," *5th International Conference on Advanced Robotics and Mechatronics (ICARM)*, pp. 178-183, 2020

[15] J. Li, Y. Zhou, J. Tan, Z. Wang, and H. Liu, "Design and Modeling of a Parallel Shifted-Routing Cable-Driven Continuum Manipulator for Endometrial Regeneration Surgery," *IEEE/RSJ International Conference on Intelligent Robots and Systems (IROS)*, pp. 3178-3183, 2020

[16] W. Shen, G. Yang, T. Zheng, Y. Wang, K. Yang, and Z. Fang, "An Accuracy Enhancement Method for a Cable-Driven Continuum Robot With a Flexible Backbone," *IEEE Access*, vol. 8, pp. 37474-37481, 2020

[17] I. A. Seleem, H. El-Hussieny, S. F. M. Assal, and H. Ishii, "Development and Stability Analysis of an Imitation Learning-Based Pose Planning Approach for Multi-Section Continuum Robot," *IEEE Access*, vol. 8, pp. 99366-99379, 2020

[18] Q. Li, H. Yang, Y. Chen, and K. Xu, "Closed Loop Control of a Continuum Surgical Manipulator for Improved Absolute Positioning Accuracy," *IEEE International Conference on Robotics and Biomimetics (ROBIO)*, pp. 1551-1556, 2019

[19] J. Lai, K. Huang, B. Lu, and H. K. Chu, "Toward Vision-based Adaptive Configuring of A Bidirectional Two-Segment Soft Continuum Manipulator," *IEEE/ASME International Conference on Advanced Intelligent Mechatronics (AIM)*, pp. 934-939, 2020

[20] H. Yang, B. Wu, X. Liu, and K. Xu, "A Closed-Loop Controller for a Continuum Surgical Manipulator Based on a Specially Designed Wrist Marker and Stereo Tracking," *IEEE/ASME International Conference on Advanced Intelligent Mechatronics (AIM)*, pp. 335-340, 2020

[21] K. Song, and H. Tsai, "Visual Servoing and Compliant Motion Control of a Continuum Robot," *18th International Conference on Control Automation and Systems (ICCAS)*, pp. 734-739, 2018

[22] H. Mo et al., "Control of a Flexible Continuum Manipulator for Laser Beam Steering," *IEEE Robotics and Automation Letters*, vol. 6, no. 2, pp. 1074-1081,2021

[23] K. Wu et al., "Safety-Enhanced Model-Free Visual Servoing for Continuum Tubular Robots Through Singularity Avoidance in Confined Environments," *IEEE Access*, vol. 7, pp. 21539-21558, 2019

[24] C. Wu, and K. Song, "Hybrid visual servoing design for a continuum robot under visibility constraint and voice commands," *16th International Conference on Control Automation and Systems (ICCAS)*, pp. 1255-1260, 2016

[25] G. Del Giudice, A. Orekhov, J. Shen, K. Joos, and N. Simaan, "Investigation of Micro-motion Kinematics of Continuum Robots for Volumetric OCT and OCT-guided Visual Servoing," *IEEE/ASME Transactions on Mechatronics*, doi: 10.1109/TMECH.2020.3043438, 2020

[26] S. Hutchinson, G. D. Hager, and P. I. Corke, "A tutorial on visual servo control," *IEEE Transactions on Robotics and Automation*, vol. 12, no. 5, pp. 651-670, 1996

[27] Robert J Webster III, and Bryan A Jones, "Design and Kinematic Modeling of Constant Curvature Continuum Robots: A Review," *The International Journal of Robotics Research*, vol 29, issue 13, pp. 1661 – 1683, 2010

[28] V. Falkenhahn, A. Hildebrandt, R. Neumann, and O. Sawodny, "Dynamic Control of the Bionic Handling Assistant," *IEEE/ASME Transactions on Mechatronics*, vol. 22, no. 1, pp. 6-17, 2017

[29] J. Canny, "A Computational Approach to Edge Detection," *IEEE Transactions on Pattern Analysis and Machine Intelligence*, vol. PAMI-8, no. 6, pp. 679-698, 1986

[30] Satoshi Suzuki, KeiichiA be, "Topological structural analysis of digitized binary images by border following," *Computer Vision, Graphics, and Image Processing*, Volume 30, Issue 1, pp. 32-46, 1985